 CMES, vol.19, no.2, pp.121-134, 2007

Molecular Mechanics Based Finite Element For Carbon Nanotube Modeling

T.C. Theodosiou[1] **and D.A. Saravanos**[2]

Abstract: In this paper a new method is introduced for carbon nanotube modeling combining features of Molecular Mechanics and Finite Element Analysis. Repetitive atomic cells are treated as finite elements, whose internal energy is determined by the semi-empirical Brenner molecular potential model; internal forces and linearized stiffness matrices are formulated analytically in order to gain in speed and accuracy, and the resultant discrete system is formulated and solved using the Newton-Raphson method. The presented method is validated through comparisons to numerical and experimental results provided by other researchers. The bending and shearing of CNTs is also simulated.

Keyword: Carbon nanotubes, molecular modeling, finite element, molecular mechanics, nanomechanics

1 Introduction

Since their discovery by Iijima [Iijima, S. (1991)] carbon nanotubes (CNTs) have attracted the interest of many scientists all over the world for their unique properties. CNTs and fullerenes in general, can be considered as a carbon allotrope like graphite and diamond. In fact, a single wall CNT (SWCNT) can be thought as a rolled-up graphene sheet. Carbon nanotubes exhibit outstanding mechanical properties with their Young modulus being around 1.2TPa [Jin and Yuan (2003)]. Depending on their exact atomic configuration, that is the geometry of the graphitic lattice, CNTs may show metallic or semi-conducting behavior [Dresselhaus, Dresselhaus and Eklund (1996); White and Mintmire (2005)]. Thus, CNTs could be used as multifunctional materials in an extremely wide range of applications. So far, there has been great effort to take advantage of the combined structural and electronic properties of the nanotubes, in order to engineer a new generation of structural materials and Nano Electro Mechanical Systems (NEMS). The former include nanocomposites [Liu and Chen (2003); Hernandez, Goze, Bernier and Rubio (1998)]; while the latter include electronics and optoelectronics [Collins and Avouris (2000); Avouris, Radosavljevic and Wind (2005)], nano-devices [Wong, Kang, Davidson and Huang (2006)], chemical and mechanical sensors [Li, Zhao, Zhu, Rodriguez, Morante, Mendoza, Poa and Silva (2006); Andzelm, Govind and Maiti (2006); Mercuri and Sgamellotti (2007); Peng, O'Keeffe, Wei, Cho, Kong, Chen, Franklin and Dai (2001)] and electromechanical actuators [Roth and Baughman (2002)]. However, many challenges remain, which should be addressed for the successful implementation of CNTs in novel bulk materials. Among them, there is a need to develop efficient analytical and numerical models which can effectively describe the mechanical behavior of CNTs in the context of envisioned applications.

There are many works reported in the area of CNT modeling which are extensively reviewed by Qian, Wagner, Liu, Yu and Ruoff (2002). In summary, there exist several classical approaches which can be used for CNT modeling based on ab-initio - or from first principles - methods [Sanchez-Portal, Artacho and Soler (1999)], tight-binding methods [Goringe, Bowleryk and Hernandez (1997)], and molecular mechanics methods [Ercolessi (1997); Brenner, Shenderova, Areshkin, Schall and Frankland (2002)]. The

[1] Mechanical Engineering and Aeronautics Dept., University of Patras, Greece

[2] Corresponding author. Applied Mechanics Section, Dept. of Mechanical & Aeronautics Engineering, University Campus, University of Patras, GR-26500, Greece. Tel.: +30-2610-992644, Fax: +30-2610-997234, email: saravanos@mech.upatras.gr

latter type of methods has become quite popular nowadays, since they are faster compared to the former ones and provide adequate accuracy. Molecular mechanics is founded on empirical or semi-empirical models for the molecular potential and internal forces of an atomistic structure, which are based on the Born-Oppenheimer approximation, which states that the energy of the system can be adequately defined by the nuclei coordinates, neglecting the electron motion. In fact, in Molecular Mechanics Models a system is analyzed by applying the macroscopic equations of motion, for example Newton's law, to the nanoworld. Several research efforts are reported in the international literature implementing Molecular Mechanics to characterize CNTs, considering several load cases, such as tension [Zhou and Shi (2002)] and buckling [Yakobson, Brabec and Berholc (1996); Yakobson and Smalley (1997)]. Multi-wall CNTs have been also modeled [Li and Chou (2003)]. A main difference among most reported works remains the type of empirical potential used. Even though Molecular Mechanics remains the fastest classical analysis method compared to ab-initio and tight-binding methods, it is still very time-consuming and requires substantial computing power. As a result, homogenization techniques have been recently developed based on extended Born rules, which treat a representative cell of atoms as an equivalent homogeneous continuous layer and use continuum mechanics finite element formulations for the CNT modeling [Xiao and Belytschko (2004); Arroyo and Belytschko (2002); Chung and Namburu (2003); Park, Cho, Kim, Jun and Im (2006)]. Other more simplified approaches have been also introduced [Li and Chou (2003)]. A summary of "Computational Nanotechnology Tools" has been published and described by Srivastava and Atluri (2002).

Between the previously mentioned two ends of available molecular mechanics and homogenization methodologies, some researchers have tried to analyze nanotubes and nanocomposites using representative cells or volumes [Liu and Chen (2002); Chakraborty (2007); Ling and Atluri (2006); Chung, Namburu and Henz (2004); Nasdala, Ernst, Legnick and Rothert (2006)]. In this regime, a new technique is introduced herein which combines elements of molecular mechanics with techniques from finite element analysis methods. The present approach takes advantage of a repetitive finite area of atoms existing in the periodic nanotube structure, which is treated as a finite element. Equivalent total and tangential stiffness matrices are directly formulated for this repetitive area, termed thereafter as "molecular finite element", using empirical molecular potential energy approximations. This is the main difference with respect to homogenization methods which use the energy of a repetitive area to calculate equivalent properties of a fictitious continuum shell, which are then used within the context of a continuum mechanics finite element formulation. The remaining of this paper describes the molecular structure of typical CNTs and the selection of a repetitive area, for which the equivalent total and linearized stiffness matrices are formulated using the Brenner-Tersoff molecular energy [Brenner (1990)]. The discrete non-linear equations of motion are formulated starting from the principle of potential energy minimization, and solved using a Newton-Raphson method. The developed molecular finite element is first used to predict the axial stretching of CNTs. Additional evaluation cases examine the bending and shearing of CNTs.

2 Molecular Configuration

As stated previously a single-wall carbon nanotube (SWCNT) can be thought as a rolled-up graphene sheet. Multi-wall CNTs (MWCNT) can be considered as an assembly of multiple SWCNTs, one positioned inside another. However, only SWCNTs are considered in this paper, and the modeling of MWCNTs is left as a future extension of this work.

A typical graphene sheet is shown in Fig. 1. Every lattice vector in the graphitic lattice can be defined in terms of two unit vectors **a**, **b**. The chiral vector $\mathbf{C}_h$ connects two crystalographically equivalent sites by declaring a pair of integers (m, n) so that,

$$\mathbf{C_h} = n\mathbf{a} + m\mathbf{b} \tag{1}$$

and its length is equal to the nanotube circumference. The angle θ formed by the chiral vector as shown also in Fig. 1 is called "chiral angle" or simply "chirality" of the nanotube.

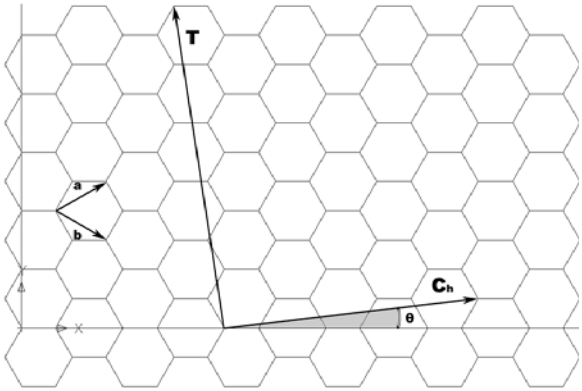

Figure 1: Graphitic lattice and primitive vectors; chiral vector $\mathbf{C_h}$ and chiral angle θ

The chirality describes the arrangement of hexagonal cells, thus, it affects every property of the nanotube including its mechanical and electrical behavior [Ivchenko, E. L.; Spivak, B. (2002)]. The nanotube diameter and chirality can be expressed in terms of (n, m) as,

$$d = \frac{\|\mathbf{C_h}\|}{\pi} = \frac{\alpha\sqrt{3}}{\pi}\sqrt{n^2+nm+n^2} \tag{2}$$

$$\theta = \tan^{-1}\left(\frac{\sqrt{3}m}{2n+m}\right) \tag{3}$$

where α is the distance between two neighboring carbon atoms. At equilibrium state, α=1.42Å approximately. Depending on the value of θ, a nanotube is termed "Zig-Zag" when $\theta = 0^o$, "Arm-Chair" when $\theta = 30^o$ and generally "Chiral" for any other value of θ between 0^o and 30^o.

3 Molecular Potential Function

In order to model the carbon nanotube, it is imperative to use an admissible molecular potential model that best describes the interactions among carbon atoms. Numerous semi-empirical models have been developed and used from time to time. Among them, we mention the famous simple model of Lennard-Jones pair potential [Jones (1924)] which describes the interaction between two covalent atoms and depends on the atomic distance, but was found to be inadequate for complex covalent systems like carbon nanotubes. Significantly better potential energy representations may be provided by a "multi-atom" model, which apply energetic penalties to any deviation of atomic bonds and angles away from their reference values [Leach, (2001)]. Brenner first proposed and latter verified by Luo, Qian, Fei, Wang and Chen (1998) that in case of graphitic structures, like carbon nanotubes, it is not necessary to consider all interatomic interactions. Instead, based on the Tersoff many-body-potential [Tersoff (1988)], Brenner suggested that stretching and bending terms are sufficient for reasonable energy approximations and provided two sets of parameter values shown in Table 1.

Table 1: Parameter sets for the Brenner Potential model

	Type I	**Type II**
Re	1.315Å	1.39Å
De	6.325eV	6.00eV
b	1.5	2.10
S	1.29	1.22
d	0.80469	0.50
R_1	1.70Å	1.70Å
R_2	2.00Å	2.00Å
a_0	0.011304	0.00020813
c_0	19.0	330.0
d_0	2.50	3.50

Both sets give the same value for the total potential and almost the same equilibrium positions, but each one may yield different stiffness values [Zhang, Huang, Geubelle, Klein and Hwang (2002)]. This result has been verified by our simulations, as well. The Brenner potential function V in its Abell-Tersoff formalism energy is expressed in terms of a repulsive potential V_R, an attractive potential V_A and a multi-body coupling term B_{ij}:

$$V = \sum_i \sum_{j>i} \left[V_R\left(r_{ij}\right) - \overline{B}_{ij} V_A\left(r_{ij}\right)\right] \tag{4}$$

The terms in the previous equation are further ex-

panded as follows:

$$V_R(r) = f_c(r) \cdot \frac{D_e}{S-1} \cdot e^{-A_1(r-R_e)} \tag{5}$$

$$V_A(r) = f_c(r) \cdot \frac{D_e \cdot S}{S-1} \cdot e^{-A_2(r-R_e)} \tag{6}$$

$$\overline{B}_{ij} = \frac{1}{2} \cdot \left(B_{ij} + B_{ji}\right) \tag{7}$$

$$B_{ij} = \left[1 + \sum_{k \neq i,j} G\left(\theta_{ijk}\right) \cdot f_c\left(r_{ik}\right)\right]^{-\delta} \tag{8}$$

$$G(\theta) = \alpha_0 \cdot \left[1 + \frac{c_0^2}{d_0^2} - \frac{c_0^2}{d_0^2 + (1+\cos\theta)^2}\right] \tag{9}$$

where: θ_{ijk} is the angle formed between position vectors $\mathbf{r}_{ij}$ and $\mathbf{r}_{ik}$; indices i, j, k indicate three different atoms of the graphitic lattice (Fig. 2); and f_c is an optional "cut-off" function and it may be used to smoothly limit the interactions in Eq. 4 within a predefined range of neighboring atoms, effectively defined by radii R_1 and R_2.

$$f_c(r) = \begin{cases} 1, & r < R_1 \\ 0.5 \cdot \left(1 + \cos\left(\pi \frac{r-R_1}{R_2-R_1}\right)\right), & R_1 < r < R_2 \\ 0, & r > R_2 \end{cases} \tag{10}$$

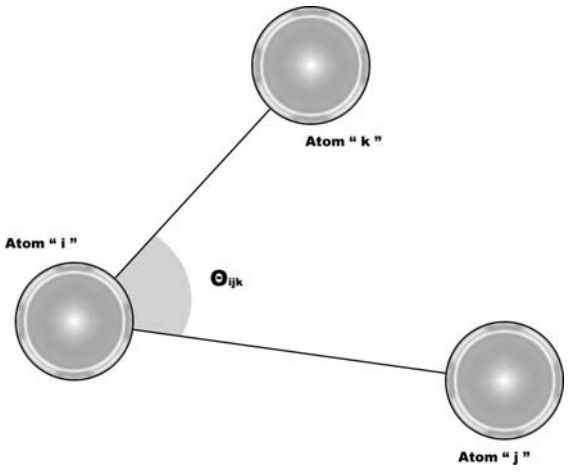

Figure 2: Definition of angle Θ_{ijk}

4 Equations of Equilibrium

A variational form of the equilibrium equations for the system of atoms in a CNT can be described as the minimization of total molecular potential energy Π:

$$\min(\Pi) = \min\left(V - \mathbf{F}^T \mathbf{u}\right) \tag{11}$$

where, V is the molecular potential of all atoms provided by Eq. (4), $\mathbf{F}$ is the vector of the externally applied forces and $\mathbf{u}$ are the displacements of all atoms in the nanotube. Using a Taylor expansion series, Eq. (11) can be expressed as:

$$\Pi = \Pi_0 + \frac{\partial \Pi}{\partial \mathbf{u}} d\mathbf{u} + \frac{1}{2} d\mathbf{u}^{\mathbf{T}} \frac{\partial^2 \Pi}{\partial \mathbf{u}^2} d\mathbf{u} + \ldots \tag{12}$$

The following notations are subsequently introduced,

$$\boldsymbol{\psi} = \frac{\partial \Pi}{\partial \mathbf{u}} \tag{13}$$

$$\left[\overline{\mathbf{K}}\right] = \frac{1}{2} \frac{\partial^2 \Pi}{\partial \mathbf{u}^2} \tag{14}$$

and Eq. (12) now can be written as,

$$\Pi = \Pi_0 + \boldsymbol{\psi}^{\mathrm{T}} d\mathbf{u} + d\mathbf{u}^{\mathrm{T}} \left[\overline{\mathbf{K}}\right] d\mathbf{u} \tag{15}$$

Substituting the potential energy expression in Eq. (15) into Eq. (13), the vector ψ is equal to:

$$\boldsymbol{\psi} = \frac{\partial \Pi}{\partial \mathbf{u}} = [\mathbf{K}]\mathbf{u} - \mathbf{F} \tag{16}$$

In the above equations, vector ψ can be considered as the imbalance vector between the internal and external atomic loads, $[\mathbf{K}] = \partial V / \partial \mathbf{u}$ as the equivalent stiffness matrix of the molecular structure and $\left[\overline{\mathbf{K}}\right]$ as the linearized (tangential) stiffness matrix. At equilibrium state, the first variation of Π diminishes, and a set of discrete nonlinear equations are obtained, which describe the balance between intermolecular and external forces on the nanotube atoms:

$$\frac{\partial \Pi}{\partial \mathbf{u}} = \boldsymbol{\psi} = [\mathbf{K}]\mathbf{u} - \mathbf{F} = \mathbf{0} \tag{17}$$

There are several ways to numerically solve the previous set of nonlinear equations and predict

the equilibrium of the nanotube after a load increment. In this paper, a Newton-Raphson iterative method was implemented. The Newton-Raphson method predicts a better estimate $d\mathbf{u}$ of the solution of either Eq. (12) or (17), by solving the following set of linear equations

$$\left[\overline{K}\right] d\mathbf{u} = -\boldsymbol{\psi} \tag{18}$$

Eq. (18) is in fact a $N \times N$ system of linear equations, where N is the total number of degrees of freedom of the nanotube. Provided that $[K]$ and $[\overline{\mathbf{K}}]$ are available, Eq. (18) can be solved and $d\mathbf{u}$ is calculated. The atomic configuration is updated using $d\mathbf{u}$ and the procedure is repeated until the magnitude of the imbalance vector ψ converges to zero. Then a new load increment is applied and a new equilibrium state, or "snapshot", of the nanotube deformation is obtained in the same manner.

5 Finite Element Approach

The governing equations and their solution procedure described in the previous section can be directly applied for the analysis of any graphitic system. However, if all atomic interactions are to be considered, the assembly and solution of Eqs. (17) and (18) become time-consuming and intractable requiring great amounts of computing power, because a great number of internal force and stiffness terms needs to be calculated for each atom. To alleviate this problem, we propose the assembly of stiffness matrices from smaller in size matrices corresponding to a finite area of the atomic nanostructure. We first make the reasonable assumption that meaningful effective atomic interactions exist only within a region of finite radius surrounding each atom. Interestingly, the assumption of a finite region of interatomic interactions is consistent with the formulation of many molecular potential models. Fig. 3 shows three such possible finite regions in the context of the Brenner potential. In this work the finite radius of interatomic interactions is assumed to be limited within the areas (1) & (2) shown in Fig. 3, which include the stretching and bending interactions in the Brenner potential. If the cut-off function is omitted, the effective range of atomic interactions will expand to include area (3), as well.

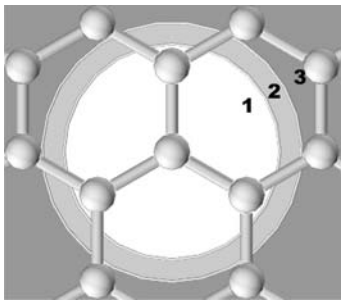

Figure 3: Effective range of the Brenner Potential: (1) Fully effective; (2) Transitional area due to the cut-off function; (3) Total effective range, if the cut-off function is omitted

As a next step, we take advantage of the repetitive atomic structure and consider the hexagonal ring of atoms shown in Fig. 4 as the repetitive finite area.

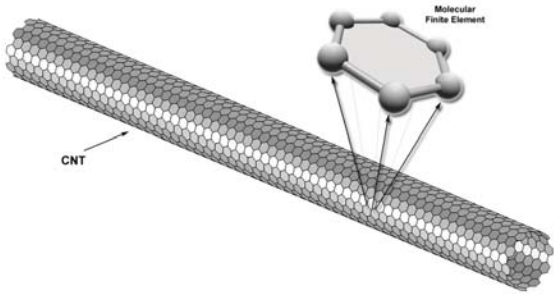

Figure 4: A CNT model assembled using the molecular finite element

Based on the two previous considerations, the area surrounded by the hexagonal ring can now be treated as a finite area whose internal energy is contributed solely by atoms belonging to the cell. If Π_e is the potential energy of all atoms in the hexagonal finite area, provided by the Brenner potential in Eq. (4), we can define the internal forces and tangential stiffness matrix of the finite area, as follows:

$$\boldsymbol{\psi}_e = \frac{\partial \Pi_e}{\partial \mathbf{u}} \tag{19}$$

$$\left[\overline{\mathbf{K}_e}\right] = \frac{1}{2}\frac{\partial^2 \Pi_e}{\partial \mathbf{u}^2} \tag{20}$$

where, subscript e indicates the finite area. The previous internal force vector and stiffness matrices are reminiscent of those in a finite element; hence the finite area can be considered as a special finite element, termed thereafter as "molecular finite element". The effect of element geometry and surface curvature of the nanotube wall are included into the element matrices through the definition of their atomic positions. Fig. 5 shows a resultant element with its nodes moved in order to comply with the nanotube geometry.

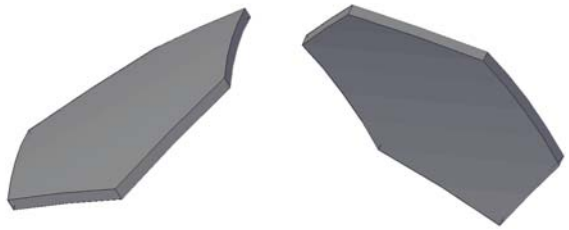

Figure 5: Two different perspective views of molecular finite element that has been adapted to conform to the nanotube wall curvature

Subsequently, the total internal force vector $[\mathbf{K}]\mathbf{u}$ and tangential stiffness matrix are synthesized from the contributions of the individual finite elements comprising the nanotube model. Thus, by limiting the calculation of stiffness into the finite area, then synthesizing the total set of governing equations as contributions of each finite element, we gain in model definition, assembly and solution time.

One novelty of this new "Finite Element" is that there is no need for the assumptions used in other successful methods, like the assumption of Periodic Boundary Conditions or the Born Rule of Homogeneous Deformation. This makes the method applicable to every carbon system. Additionally, the implementation of FE Analysis features facilitates the computational solution and parallelization of the analysis code which substantially minimizes the required solution time. Another advantage is that this element makes feasible the investigation of local effects, like defects, without disturbing the whole system. The presence of defective rings, like pentagon-rings, can be modeled by isolating the appropriate atoms of the Finite Element. Alternatively, the presence of defects in a nanotube can be modeled by modifying or simply eliminating individual elements.

6 Equivalent continuum response - Postcalculation

After the numeric solution of the CNT response has been completed, data is collected and postprocessed, in order to retrieve the macroscopic equivalent mechanical response of a section of the nanotube. As the deformation and total potential energy of the full system is known for each load increment, one may calculate the corresponding measures for stress and strain. Based on the deformation, the "deformation gradient" [**F**] can be calculated as [Xiao and Belytschko (2004); Arroyo and Belytschko (2002)]:

$$[\mathbf{F}] = \frac{\partial \mathbf{u}}{\partial \mathbf{U}} \tag{21}$$

In Eq. (21) **u** denotes the atomic configuration, i.e. the Cartesian coordinates of the atoms, at any deformed snapshot, and **U** denotes the initial equilibrium configuration. Then, the Lagrange-Green strain tensor can be calculated through the equation:

$$\varepsilon = \frac{1}{2}\left[\mathbf{F}^{\mathrm{T}}\mathbf{F} - \mathbf{I}\right] \tag{22}$$

where [**I**] is the identity tensor.

The stress tensor $[\sigma]$ can be found as:

$$\sigma_{ij} = \frac{1}{\Omega_0}\frac{\partial^2 \Pi}{\partial \varepsilon_{ij}^2} \tag{23}$$

where, $\Omega_0 = A_0 \cdot t$ is the volume of the undeformed nanotube, t denotes the wall thickness and A_0 is the initial equilibrium area of the nanotube section. A reasonable estimate for t is the interlayer distance of graphite, that is t=0.34nm. Dividing stress by strain yields to the elastic moduli of the nanotube. For instance the longitudinal elasticity modulus and the equivalent Poisson ratio are given by:

$$E_{xx} = \frac{\sigma_{xx}}{\varepsilon_{xx}} \quad \text{and} \quad \nu = -\frac{\varepsilon_{trans}}{\varepsilon_{xx}} \tag{24}$$

In the previous equation, ε_{xx} is the longitudinal strain and ε_{trans} is the strain in the transverse direction at the middle of the nanotube.

7 Validations

In order to evaluate the response of the novel finite element, its results were validated through comparisons with theoretical and experimental data obtained from the open literature on CNTs. A prototype code was developed and run on a parallel processing system consisting of 8 Pentium-4 class CPUs.

In each simulation a standard procedure has been followed, in order to obtain repeatable results. Firstly, the Cartesian coordinates of the carbon atoms were defined for a specific nanotube configuration based on Eqs 1, 2 & 3 and a finite element CNT model is assembled using the molecular finite element presented previously. Unless otherwise stated, in most cases a length-to-diameter ratio above 5.5 has been used for reasons explained later in this paper. Boundary conditions and loads were applied appropriately depending on the case studied, always a few Å away from the tube ends in order to avoid local boundary effects. The loads were applied incrementally using a predefined number of load steps. Due to accuracy errors in the initial carbon-carbon distance, some relaxation steps where required in order to achieve initial equilibrium prior to loading and maximum accuracy in the equivalent property postcalculation. Both Type-I and Type-II Brenner models were tried in the present method, but the Type-II model was found to lead to more accurate numerical predictions, thus it was subsequently used in all numerical results shown herein.

The method was first tested for the simple case of calculating the equilibrium state of an unloaded plain graphene sheet. A graphite sheet was modeled using approximate values for the carbon-carbon distance. One edge of the sheet was clamped and the relaxation of the system was predicted. After relaxation, the equilibrium distance between neighboring carbon atoms was predicted to be 1.4201Å which is very close to the experimentally observed value of 1.419Å.

Subsequently, several open nanotube configurations were subjected to uniaxial tension in order to estimate the equivalent Young modulus. One end of the nanotube was clamped and the other was loaded by forcing uniform atomic displacements to a ring of atoms near the other end. The equivalent strain and properties were calculated based on the predicted deformation of a finite length of the CNT atoms away from the ends (Fig. 6) to avoid edge-effects.

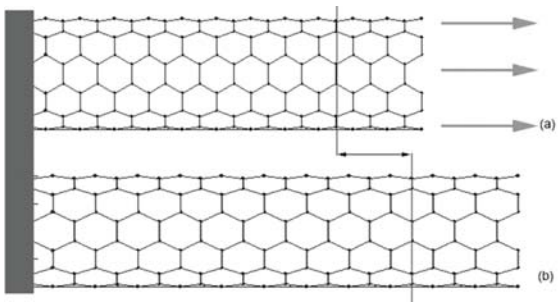

Figure 6: Predicted CNT deformation subject to axial loading. (a) Initial unloaded equilibrium state; (b) predicted deformed shape. The approximate location of points used for the postcalculation of equivalent strains and properties is also shown.

Numerical results obtained by the present method are compared with results reported by Jin and Yuan (2003), who provided a list of elastic properties for several nanotube configurations based on molecular dynamics simulations. Details about the models of these simulations are presented in Table 2.

Table 2: CNT model parameters

Tube Type	Atoms	Elements	Diameter (Å)	Length (Å)
(6,6)	456	216	8.14	45.60
(7,7)	616	294	9.49	53.01
(8,8)	800	384	10.85	60.40
(9,9)	1008	486	12.20	67.79
(10,10)	1240	600	13.56	75.02

Jin and Yuan's model configurations were replicated and analyzed using the presented method and the results are shown in Table 3. Unlike Yuan's model, which gives almost the same value for E in all cases, our method predicts a decrease

in E as the diameter of the nanotube grows; this appears to be expected, since for an infinite radius, the Young modulus should approach the modulus value of graphite (approximately 1.1TPa).

The predicted numerical results, also fall within the range of reported values obtained either by other simulation methods or experimentally observed. Grigoras, Gusev, Santos and Suter (2002) estimated E=1.07TPa using both Molecular Dynamics and Monte Carlo simulations. Treacy, Ebbesen and Gibson (1996) obtained a Young modulus of 1.8±0.9TPa, while Krishnan, Dujardin, Ebbesen, Yannilos and Treacy (1998) estimated the stiffness of SWCNTs to be around 1.3TPa using Transmission Electron Microscopy.

Table 3: Predicted equivalent axial modulus of a single wall nanotube

	CNT configuration				
Predicted modulus E(TPa)	**(6,6)**	**(7,7)**	**(8,8)**	**(9,9)**	**(10,10)**
Jin and Yuan (2003)	1.324	1.336	1.339	1.335	1.338
Present work	1.355	1.312	1.326	1.302	1.260
Difference (%)	2.3	1.8	0.9	2.5	5.8

It seems that the predicted values are very sensitive to the potential model used and less sensitive to the chirality of the nanotube. Variations among various researchers may occur due to (i) the selection of different modelling techniques; (ii) the applied loading and boundary conditions; and (iii) the implemented numerical method for the solutions of Eq. 18. The selections of these three factors determine the overall accuracy and effectiveness of the method. Nevertheless, the results obtained by our simulation method are in very good agreement with the results of other research studies, and certainly within a reasonably acceptable range.

8 Application Cases

Apart from the simple extension cases presented above, several more complex cases were also modeled. Firstly, the effect of the length-to-diameter aspect ratio (L/d) on the CNT extensional response was studied. Several CNT models of the same type but of different aspect ratios were analyzed using the described procedure. As shown in Fig. 7, the predicted curves of the equivalent stress and strain properties have significant irregularities for small ratios, but seem to converge for L/d values over 5.

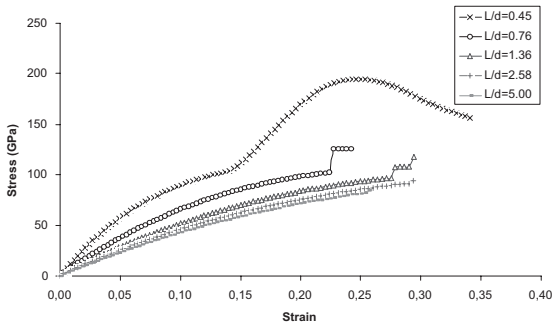

Figure 7: The equivalent stress-strain response of a CNT subject to tension for various length-to-diameter (L/d) ratios

The results suggest that nanotube models with ratios $L/d > 5$ can be used to extract information regarding equivalent tensile properties of a CNT. It is also observed that the CNT behaves nonlinearly, thus the equivalent tangential elastic coefficients will depend on the applied stress-strain value. The axial Young moduli values estimated in the previous cases (Table 3) were calculated at low strain ($\varepsilon \approx 0$). Fig. 8 presents the mean value of the energy stored in a hexagonal cell at the unloaded equilibrium state for several CNT types.

It seems that the higher the radius, the lower is the energy stored in the cell, which means that the atomic structure is more stable. This makes sense because the lowest energy level and of course the most stable structure should correspond to an infinitely large radius, this is a plain graphene sheet.

The bending of CNTs was also studied. The nanotube was modeled in the same way as in the case of uniaxial tension, but the load was applied in a manner that resembles pure bending. Selected atoms near both ends of the CNT were displaced such that both CNT ends were counter-

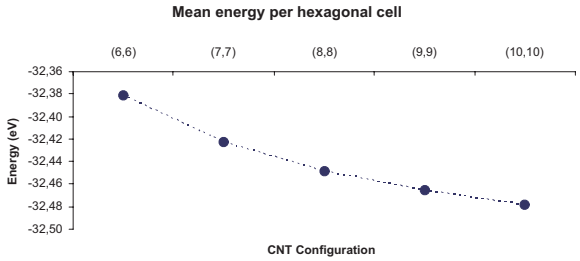

Figure 8: Effect of the CNT configuration on the average value of energy stored in each hexagonal cell

rotated around parallel lateral axes. The bending load was incrementally applied until the tangential stiffness matrix became singular. The singularity of the linearized stiffness matrix can be viewed as a probable indication of buckling instability or an atomic failure in the molecular structure of the CNT. However, what physically happens near and beyond this "critical load" exceeds the scope of the current study and will be considered as a future extension of this work.

In order to obtain some sensitivity of the response to defects in its molecular structure, the model was further modified in order to represent a "defective" geometry; this was done by removing some finite elements at the middle of the CNT. The simulation was performed again and the results were compared to the ones concerning the undamaged nanotube. The final snapshots are shown in Fig. 9.

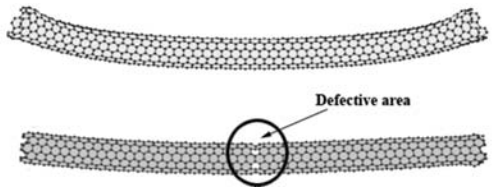

Figure 9: Predicted CNT deformations subjected to bending at the state where the tangential stiffness matrix becomes singular. (a) Undamaged CNT; (b) CNT with defects, for which singularity of the tangential stiffness matrix occurs much earlier

As expected, the critical bending load for the defective CNT was found to be much less than the critical load of the undamaged one.

Similarly, a shearing case was modeled. Transverse loading was applied incrementally until the tangential stiffness matrix became singular. At the corresponding final load step, the expected deformed shape is shown in Fig. 10.

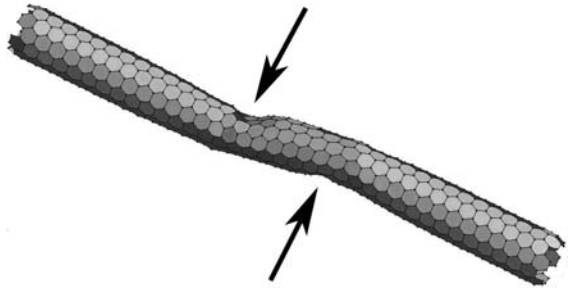

Figure 10: Deformed CNT subject to a pair of shearing displacements

Some local buckling effects can also be observed in this figure.

In closing, the numerical simulations illustrated that this novel method and finite element can predict the response of SWCNTs subjected to a variety of mechanical loads, both accurately and effectively, thus providing a fast and accurate tool for nanotube modelling and extraction of CNT properties.

9 Summary

A new method for analyzing the mechanical response of carbon nanotubes has been described in this paper. It combines features from existing successful methods of Molecular Mechanics and Finite Element formulations, resulting to effective treatments of a cell of atoms as a Molecular Finite Element. A great novelty of this new method is that there is no need for assuming periodic boundary conditions or homogeneous deformations, thus, it can be implemented for modeling CNTs of finite length, configurations with complex geometries, or local effects in regions where the limits of homogeneity assumptions are exceeded.

Validation cases have accurately predicted the effect of CNT configurations and aspect ratio (L/d) on the CNT mechanical response and properties. More complex loading cases, such as bending and shearing, have been also modeled and simulated. The effect of defects and damage on the CNT response was also captured. The developed prototype code has been taking advantage of the parallelization features of FEA solvers, and was used on parallel processing systems reducing the required solution time. Future work will address the modelling of multi wall CNTs.

Acknowledgement: Part of this work was funded by the Research Committee of the University of Patras through the "K. Karatheodori" Research Program. The authors gratefully acknowledge this support.

References

Andzelm, J.; Govind, N.; Maiti, A. (2006): Nanotube-based gas sensors – Role of structural defects, *Chemical Physics Letters*, vol. 421, pp. 58–62

Arroyo, M.; Belytschko, T. (2002): An atomistic-based finite deformation membrane for single layer crystalline films, *Journal of the Mechanics and Physics of Solids*, vol. 50, pp. 1941-1977

Avouris, P.; Radosavljevic, M.; Wind, S. J. (2005): Carbon nanotube electronics and optoelectronics, *Springer verlag*

Brenner, D. W. (1990): Empirical potential for hydrocarbons for use in simulating the chemical vapor decomposition of diamond films, *Physical Review B*, vol. 42, pp. 15

Brenner, D. W.; Shenderova, O. A.; Areshkin, D. A.; Schall, J. D.; Frankland, S.-J. V. (2002): Atomic modeling of carbon-based nanostructures as a tool for developing new materials and technologies, *CMES: Computer Modeling in Engineering & Sciences,* vol. 3, no. 5, pp. 643-673

Chakraborty, A. (2007): Shell element based model for wave propagation analysis in multi-wall carbon nanotubes, *International Journal of Solids and Structures*, vol. 44, pp. 1628–1642

Chung, P. W.; Namburu, R. R. (2003): On a formulation for a multiscale atomistic-continuum homogenization method, *International Journal of Solids and Structures*, vol. 40, pp. 2563-2588

Chung, P. W., Namburu, R. R., Henz, B. J. (2004): A lattice statics-based tangent-stiffness finite element method, *CMES: Computer Modeling in Engineering & Sciences,* vol. 5, no. 1, pp. 45-62

Collins, P. G.; Avouris, P. (2000): Nanotubes for electronics, *Sci. Amer.*, vol. 283, pp. 38–45

Dresselhaus, M. S.; Dresselhaus, G.; Eklund, P. C. (1996): Science of fullerenes and carbon nanotubes, *Academic Press*, San Diego

Ercolessi, F. (1997): A molecular dynamics primer, *Spring College in computational physics*, ICTP, Trieste

Goringe, C. M.;. Bowleryk, D. R.; Hernandez, E. (1997): Tight-binding modelling of materials, *Rep. Prog. Phys.*, vol. 60, pp. 1447-1512

Grigoras, S.; Gusev, A. A.; Santos, S.; Suter, U. W. (2002): Evaluation of the elastics constants of nanoparticles from atomistic simulations, *Polymer*, vol. 43, pp. 489-494

Hernandez, E.; Goze, C. Bernier, P.; Rubio, A. (1998): Elastic properties of C and CxByNz composite nanotubes, *Phys. Rev. Lett.*, vol. 80, pp. 4502-4505

Iijima, S. (1991): Helical microtubules of graphitic carbon. *Nature*, vol. 354, pp. 56-58

Ivchenko, E. L.; Spivak, B. (2002): Chirality effects in carbon nanotubes, *Physical Review B*, vol. 66, pp. 155404

Krishnan, A.; Dujardin, E.; Ebbesen, T. W.; Yannilos, P. N.; Treacy, M. M. J. (1998): Young's modulus of single-walled nanotubes, *Phys. Rev. B*, vol. 58, pp. 14013

Jin, Y.; Yuan, F. G. (2003): Simulation of elastic properties of single-walled carbon nanotubes, *Composites Science and Technology*, vol. 63, pp. 1507-1515

Jones, J. E. (1924): On the determination of molecular fields-I: From the variation of viscosity of a gas with temperature, *Proc. Roy. Soc.*, vol. 106, pp. 441

Jones, J. E. (1924): On the determination of molecular fields-II: From the equations of state of gas, *Proc. Roy. Soc.*, vol. 106, pp. 463

Leach, A. (2001): Molecular modelling: principles and applications, Prentice Hall 2001

Li, C.; Chou, T. W. (2003): A structural mechanics approach for the analysis of carbon nanotubes, *International Journal of Solids and Structures*, vol. 40, pp. 2487-2499

Li, C.; Chou, T. W. (2003): Elastic moduli of multi-walled carbon nanotubes and the effect of van der Waals forces, *Composites Science and Technology*, vol. 63, pp. 1517-1524

Li, Y. H.; Zhao, Y. M.; Zhu, Y. Q.; Rodriguez, J.; Morante, J. R.; Mendoza, E.; Poa, C. H. P.; Silva, S. R. P. (2006): Mechanical and NH_3 sensing properties of long multi-walled carbon nanotube ropes, *Carbon*, vol. 44, pp. 1821–1825

Ling, X.; Atluri, S. N. (2006): A lattice-based cell model for calculating thermal capacity and expansion of single wall carbon nanotubes, *CMES: Computer Modeling in Engineering & Sciences,* vol. 14, no. 2, pp. 91-100

Liu, Y. J.; Chen, X. L. (2003): Evaluations of the effective material properties of carbon nanotubes based composites using a nanoscale representative volume element, *Mechanics of materials*, vol. 35, pp. 69-81

Luo, X.; Qian, G.; Fei, W.; Wang, E, G.; Chen, C. (1998): Systematic study for β-SiC surface structures by molecular dynamics simulations, *Physical Review B*, vol. 57, No 14

Mercuri, F; Sgamellotti, A. (2007): Theoretical investigations on the functionalization of carbon nanotubes, *Inorganica Chimica Acta*, vol. 360, pp. 785–793

Nasdala, L.; Ernst, G.; Legnick, M.; Rothert, H. (2005): Finite element analysis of carbon nanotubes with Stone-Wales defects, *CMES: Computer Modeling in Engineering & Sciences,* vol. 7, no. 3, pp. 293-304

Park, J. J.; Cho, Y.-S.; Kim, S. Y.; Jun, S.; Im, S. (2006): A quasi-continuum method for deformations of carbon nanotubes, *CMES: Computer Modeling in Engineering & Sciences,* vol. 11, no. 2, pp. 61-72

Peng, S.; O'Keeffe, J., Wei, C.; Cho, K.; Kong, J.; Chen, R.; Franklin, N.; Dai, H. (2001): Carbon nanotube chemical and mechanical sensors, *Conference Paper for the 3rd International Workshop on Structural Health Monitoring*

Qian, D.; Wagner, G. J.; Liu, W. K.; Yu, M. F.; Ruoff, R. S. (2002): Mechanics of carbon nanotubes, *Appl. Mech. Rev.*, vol. 55, No 6

Roth, S.; Baughman, R. H. (2002): Actuators of individual carbon nanotubes, *Current Applied Physics*, vol. 2, pp. 311–314

Sanchez-Portal, D.; Artacho, E.; Soler, J. M. (1999): Ab initio structural, elastic, and vibrational properties of carbon nanotubes, *Phys. Rev. B*, vol. 59, pp. 12678

Srivastava, D.; Atluri, S. N. (2002): Computational Nanotechnology: A Current Perspective, *CMES: Computer Modeling in Engineering & Sciences,* vol. 3, no. 5, pp. 531-538

Tersoff, J. (1988): Empirical interatomic potential for carbon with applications to amorphous carbon, *Phys. Lett.*, vol. 61, pp. 2879

Treacy, M. M. J.; Ebbesen, T. W.; Gibson, J. M. (1996): Exceptionally high Young's modulus observed for individual carbon nanotubes, *Nature*, vol. 381, pp. 678-680

White, C. T.; Mintmire, J. W. (2005): Fundamental properties of single-wall carbon nanotubes, *J. Phys. Chem. B,* vol. 109, pp. 52-65

Wong, Y. M.; Kang, W. P.; Davidson, J. L.; Huang, J. H. (2006): Carbon nanotubes field emission integrated triode amplifier array, Diamond & Related Materials, vol. 15, pp. 1990–1993

Xiao, S. P.; Belytschko T. (2004): A bridging domain method for coupling continua with molecular dynamics, *Comput. Methods Appl. Mech. Engrg.*, vol. 193, pp. 1645-1669

Yakobson, B. I.; Brabec, C. J.; Berholc, J. (1996): Nanomechanics of carbon tubes: Instabilities beyond linear response, *Phys. Rev. Lett.*, vol. 76, pp. 2511-2514

Yakobson, B. I.; Smalley, R. E. (1997): Fullerene nanotubes: C-1000000 and beyond,

Am. Sci., vol. 85, pp. 324-327

Zhang, P.; Huang, Y.; Geubelle, P. H.; Klein, P. A.; Hwang, K. C. (2002): The elastic modulus of single-wall carbon nanotubes: a continuum analysis incorporating interatomic potentials, *International Journal of Solids and Structures*, vol. 39, pp.3893-3906

Zhou, L. G.; Shi, S. Q. (2002): Molecular dynamics simulations on tensile mechanical properties of single-walled carbon nanotubes with and without hydrogen storage, *Computational Materials Science*, vol. 23, pp. 166-174

Appendix: Analytical expressions for the imbalance vector ψ and the tangential stiffness matrix $\left[\overline{K}\right]$

Atomic position vector of the i^{th} atom:

$$\mathbf{r_i} = \begin{Bmatrix} u_{i1} \\ u_{i2} \\ u_{i3} \end{Bmatrix} \tag{25}$$

Relative atomic positions between atoms i and j:

$$\mathbf{r}_{ij} = \mathbf{r_j} - \mathbf{r_i} \tag{26}$$

Norm of the relative position vector:

$$r_{ij} = \left\| \mathbf{r_{ij}} \right\| \tag{27}$$

Imbalance Vector ψ

$$\frac{\partial r_{ij}}{\partial u_k} = \begin{cases} \frac{u_{ik}-u_{jk}}{r_{ij}}, & k = i \\ \frac{u_{jk}-u_{ik}}{r_{ij}}, & k = j \\ 0, & \text{otherwise} \end{cases} \tag{28}$$

$$\frac{\partial F_C\left(r_{ij}\right)}{\partial r_{ij}} = \begin{cases} 0, & r < R_1 \\ -0.5 \cdot \frac{\pi}{R_1 - R_2} \cdot \sin\left(1 + \pi \cdot \frac{r-R_1}{R_1-R_2}\right), & R_1 \le r < R_2 \\ 0, & R_2 \le r \end{cases} \tag{29}$$

$$\frac{\partial F_C\left(r_{ij}\right)}{\partial u_k} = \frac{\partial F_C\left(r_{ij}\right)}{\partial r_{ij}} \cdot \frac{\partial r_{ij}}{\partial u_k} \tag{30}$$

$$\frac{\partial V_R\left(r_{ij}\right)}{\partial r_{ij}} = \left[\frac{\partial F_C\left(r_{ij}\right)}{\partial r_{ij}} - F_C\left(r_{ij}\right) \cdot A_1\right] \cdot \frac{D_e}{S-1} \cdot e^{-A_1 \cdot (r - R_e)} \tag{31}$$

$$\frac{\partial V_A\left(r_{ij}\right)}{\partial r_{ij}} = \left[\frac{\partial F_C\left(r_{ij}\right)}{\partial r_{ij}} - F_C\left(r_{ij}\right) \cdot A_2\right] \cdot \frac{D_e \cdot S}{S-1} \cdot e^{-A_2 \cdot (r - R_e)} \tag{32}$$

$$\frac{\partial V_R\left(r_{ij}\right)}{\partial u_k} = \frac{\partial V_R\left(r_{ij}\right)}{\partial r_{ij}} \cdot \frac{\partial r_{ij}}{\partial u_k} \tag{33}$$

$$\frac{\partial V_A\left(r_{ij}\right)}{\partial u_k} = \frac{\partial V_A\left(r_{ij}\right)}{\partial r_{ij}} \cdot \frac{\partial r_{ij}}{\partial u_k} \tag{34}$$

$$\frac{\partial G(\theta)}{\partial \cos\theta} = \frac{2 a_0 c_0 (1 + \cos\theta)}{\left[d_0^2 + (1+\cos\theta)^2\right]^2} \tag{35}$$

$$\frac{\partial \mathbf{r_{ij}}}{\partial u_k} = \begin{cases} -\widehat{\mathbf{u_k}}, & k = i \\ \widehat{\mathbf{u_k}}, & k = j \\ 0, & \text{otherwise} \end{cases} \tag{36}$$

$$\frac{\partial}{\partial u_k}\left(\frac{1}{r_{ij}}\right) = -\frac{\partial r_{ij}}{\partial u_k} \cdot \left(\frac{1}{r_{ij}}\right)^2 \tag{37}$$

$$\frac{\partial \cos\left(\theta_{ijk}\right)}{\partial u_m} = \frac{1}{r_{ij} \cdot r_{ik}} \cdot \mathbf{r_{ik}} \cdot \frac{\partial \mathbf{r_{ij}}}{\partial u_m} + \frac{1}{r_{ij} \cdot r_{ik}} \cdot \mathbf{r_{ij}} \cdot \frac{\partial \mathbf{r_{ij}}}{\partial u_m} + \frac{1}{r_{ik}} \cdot \mathbf{r_{ij}} \cdot \mathbf{r_{ik}} \cdot \frac{\partial}{\partial u_m}\left(\frac{1}{r_{ij}}\right) + \frac{1}{r_{ij}} \cdot \mathbf{r_{ij}} \cdot \mathbf{r_{ik}} \cdot \frac{\partial}{\partial u_m}\left(\frac{1}{r_{ik}}\right) \tag{38}$$

$$\frac{\partial G\left(\theta_{ijk}\right)}{\partial u_m} = \frac{\partial G\left(\theta_{ijk}\right)}{\partial \cos\theta_{ijk}} \cdot \frac{\partial \cos\theta_{ijk}}{\partial u_m} \tag{39}$$

$$\frac{\partial B_{ij}}{\partial u_m} = -\delta \cdot B_{ij}^{1+\frac{1}{\delta}} \cdot \sum_{k \neq i,j} \left[\frac{\partial G\left(\theta_{ijk}\right)}{\partial u_m} \cdot F_C\left(r_{ik}\right) + G\left(\theta_{ijk}\right) \cdot \frac{\partial F_C\left(r_{ik}\right)}{\partial u_m}\right] \tag{40}$$

$$\frac{\partial \overline{B_{ij}}}{\partial u_k} = 0.5 \cdot \left(\frac{\partial B_{ij}}{\partial u_k} + \frac{\partial B_{ji}}{\partial u_k} \right) \tag{41}$$

$$\frac{\partial V}{\partial u_k} = \sum_i \sum_{j>i} \left[\frac{\partial V_R\left(r_{ij}\right)}{\partial u_k} - \overline{B_{ij}} \cdot \frac{\partial V_A\left(r_{ij}\right)}{\partial u_k} - \frac{\partial B_{ij}}{\partial u_k} \cdot V_A\left(r_{ij}\right) \right] \tag{42}$$

$$\boldsymbol{\psi} = \frac{\partial \Pi}{\partial \mathbf{u}} = \frac{\partial}{\partial \mathbf{u}} \left(V - \mathbf{F^T} \cdot \mathbf{u} \right) \tag{43}$$

If a constant force field is applied on the system, Eq. (43) may be reduced to Eq. (42), therefore

$$\boldsymbol{\psi} = \sum_i \sum_{j>i} \left[\frac{\partial V_R\left(r_{ij}\right)}{\partial u_k} - \overline{B_{ij}} \cdot \frac{\partial V_A\left(r_{ij}\right)}{\partial u_k} - \frac{\partial B_{ij}}{\partial u_k} \cdot V_A\left(r_{ij}\right) \right], \quad k = 1...N \tag{44}$$

Tangential Stiffness Matrix $\left[\overline{K}\right]$

$$\frac{\partial^2 F_C\left(r_{ij}\right)}{\partial r_{ij}^2} = \begin{cases} 0, & r < R_1 \\ -0.5 \cdot \left(\frac{\pi}{R_1 - R_2}\right)^2 \cdot \cos\left(\pi \cdot \frac{r - R_1}{R_1 - R_2}\right), & R_1 \le r < R_2 \\ 0, & R_2 \le r \end{cases} \tag{45}$$

$$\frac{\partial^2 F_C\left(r_{ij}\right)}{\partial u_p \partial u_q} = \frac{\partial^2 F_C\left(r_{ij}\right)}{\partial r_{ij}^2} \cdot \frac{\partial r_{ij}}{\partial u_p} \cdot \frac{\partial r_{ij}}{\partial u_q} \tag{46}$$

$$\frac{\partial^2 V_R\left(r_{ij}\right)}{\partial r_{ij}^2} = \left[\frac{\partial^2 F_C\left(r_{ij}\right)}{\partial r_{ij}^2} - 2 \cdot A_1 \cdot \frac{\partial F_C\left(r_{ij}\right)}{\partial r_{ij}} + A_1^2 \cdot F_C\left(r_{ij}\right) \right] \cdot \frac{D_e}{S-1} \cdot e^{-A_1 \cdot (r - R_e)} \tag{47}$$

$$\frac{\partial^2 V_R\left(r_{ij}\right)}{\partial u_p \partial u_q} = \frac{\partial^2 V_R\left(r_{ij}\right)}{\partial r_{ij}^2} \cdot \frac{\partial r_{ij}}{\partial u_p} \cdot \frac{\partial r_{ij}}{\partial u_p} + \frac{\partial V_R\left(r_{ij}\right)}{\partial r_{ij}} \cdot \frac{\partial^2 r_{ij}}{\partial u_p \partial u_q} \tag{48}$$

$$\frac{\partial^2 V_A\left(r_{ij}\right)}{\partial r_{ij}^2} = \left[\frac{\partial^2 F_C\left(r_{ij}\right)}{\partial r_{ij}^2} - 2 \cdot A_2 \cdot \frac{\partial F_C\left(r_{ij}\right)}{\partial r_{ij}} + A_2^2 \cdot F_C\left(r_{ij}\right) \right] \cdot \frac{D_e \cdot S}{S-1} \cdot e^{-A_2 \cdot (r - R_e)} \tag{49}$$

$$\frac{\partial^2 V_A\left(r_{ij}\right)}{\partial u_p \partial u_q} = \frac{\partial^2 V_A\left(r_{ij}\right)}{\partial r_{ij}^2} \cdot \frac{\partial r_{ij}}{\partial u_p} \cdot \frac{\partial r_{ij}}{\partial u_p} + \frac{\partial V_A\left(r_{ij}\right)}{\partial r_{ij}} \cdot \frac{\partial^2 r_{ij}}{\partial u_p \partial u_q} \tag{50}$$

$$\begin{aligned} \frac{\partial^2 \cos\left(\theta_{ijk}\right)}{\partial u_p \partial u_q} &= \frac{1}{r_{ij} \cdot r_{ik}} \cdot \frac{\partial r_{ij}}{\partial u_p} \cdot \frac{\partial r_{ik}}{\partial u_q} \\ &+ \frac{1}{r_{ik}} \cdot \mathbf{r_{ik}} \cdot \frac{\partial \mathbf{r_{ij}}}{\partial u_p} \cdot \frac{\partial}{\partial u_q}\left(\frac{1}{r_{ij}}\right) \\ &+ \frac{1}{r_{ij}} \cdot \mathbf{r_{ik}} \cdot \frac{\partial \mathbf{r_{ij}}}{\partial u_p} \cdot \frac{\partial}{\partial u_q}\left(\frac{1}{r_{ik}}\right) \\ &+ \frac{1}{r_{ij} \cdot r_{ik}} \cdot \frac{\partial \mathbf{r_{ik}}}{\partial u_p} \cdot \frac{\partial \mathbf{r_{ij}}}{\partial u_q} \\ &+ \frac{1}{r_{ik}} \cdot \mathbf{r_{ij}} \cdot \frac{\partial \mathbf{r_{ik}}}{\partial u_p} \cdot \frac{\partial}{\partial u_q}\left(\frac{1}{r_{ij}}\right) \\ &+ \frac{1}{r_{ij}} \cdot \mathbf{r_{ij}} \cdot \frac{\partial \mathbf{r_{ik}}}{\partial u_p} \cdot \frac{\partial}{\partial u_q}\left(\frac{1}{r_{ik}}\right) \\ &+ \frac{1}{r_{ik}} \cdot \mathbf{r_{ik}} \cdot \frac{\partial \mathbf{r_{ij}}}{\partial u_q} \cdot \frac{\partial}{\partial u_p}\left(\frac{1}{r_{ij}}\right) \\ &+ \frac{1}{r_{ik}} \cdot \mathbf{r_{ij}} \cdot \frac{\partial \mathbf{r_{ik}}}{\partial u_q} \cdot \frac{\partial}{\partial u_p}\left(\frac{1}{r_{ij}}\right) \\ &+ \frac{1}{r_{ik}} \cdot \mathbf{r_{ij}} \cdot \mathbf{r_{ik}} \cdot \frac{\partial^2 r_{ij}}{\partial u_p \partial u_q} \\ &+ \mathbf{r_{ij}} \cdot \mathbf{r_{ik}} \cdot \frac{\partial}{\partial u_p}\left(\frac{1}{r_{ij}}\right) \cdot \frac{\partial}{\partial u_q}\left(\frac{1}{r_{ik}}\right) \\ &+ \frac{1}{r_{ij}} \cdot \mathbf{r_{ik}} \cdot \frac{\partial \mathbf{r_{ij}}}{\partial u_q} \cdot \frac{\partial}{\partial u_p}\left(\frac{1}{r_{ik}}\right) \end{aligned} \tag{51}$$

$$+\frac{1}{r_{ij}}\cdot\mathbf{r_{ij}}\cdot\frac{\partial\mathbf{r_{ik}}}{\partial u_p}\cdot\frac{\partial}{\partial u_p}\left(\frac{1}{r_{ik}}\right)$$
$$+\frac{1}{r_{ij}}\cdot\mathbf{r_{ij}}\cdot\mathbf{r_{ik}}\cdot\frac{\partial^2 r_{ik}}{\partial u_p\partial u_q}$$
$$+\mathbf{r_{ij}}\cdot\mathbf{r_{ik}}\cdot\frac{\partial}{\partial u_p}\left(\frac{1}{r_{ik}}\right)\cdot\frac{\partial}{\partial u_q}\left(\frac{1}{r_{ij}}\right)$$

$$\frac{\partial^2 G\left(\theta_{ijk}\right)}{\partial u_p\partial u_q}=\frac{-2\cdot a_0\cdot c_0^2\cdot\left[3\cdot\left(1+\cos\theta_{ijk}\right)^2-d_0^2\right]}{\left[d_0^2+\left(1+\cos\theta_{ijk}\right)^2\right]^3}$$
$$\cdot\frac{\partial\cos\theta_{ijk}}{\partial u_p}\cdot\frac{\partial\cos\theta_{ijk}}{\partial u_q}+\frac{\partial G\left(\theta_{ijk}\right)}{\partial\cos\theta_{ijk}}\cdot\frac{\partial^2\cos\theta_{ijk}}{\partial u_p\partial u_q} \quad (52)$$

$$\frac{\partial^2 B_{ij}}{\partial u_p\partial u_q}=-\delta\cdot\left(1+\frac{1}{\delta}\right)\cdot B_{ij}^{\frac{1}{\delta}}\cdot\frac{\partial B_{ij}}{\partial u_q}$$
$$\cdot\sum_{k\neq i,j}\left[\frac{\partial F_C\left(r_{ik}\right)}{\partial u_p}\cdot G\left(\theta_{ijk}\right)+F_C\left(r_{ik}\right)\cdot\frac{\partial G\left(\theta_{ijk}\right)}{\partial u_p}\right]$$
$$+(-\delta)\cdot B_{ij}^{1+\frac{1}{\delta}}\cdot\sum_{k\neq i,j}\left[\frac{\partial^2 F_C\left(r_{ik}\right)}{\partial u_p\partial u_q}\cdot G\left(\theta_{ijk}\right)\right.$$
$$+\frac{\partial F_C\left(r_{ik}\right)}{\partial u_p}\cdot\frac{\partial G\left(\theta_{ijk}\right)}{\partial u_q}+\frac{\partial F_C\left(r_{ik}\right)}{\partial u_q}\cdot\frac{\partial G\left(\theta_{ijk}\right)}{\partial u_p}$$
$$\left.+F_C\left(r_{ik}\right)\cdot\frac{\partial^2 G\left(\theta_{ijk}\right)}{\partial u_p\partial u_q}\right] \quad (53)$$

$$\frac{\partial^2 V}{\partial u_p\partial u_q}=$$
$$\sum_{k\neq i,j}\left[\frac{\partial^2 V_R\left(r_{ij}\right)}{\partial u_p\partial u_q}-0.5\cdot\left(\frac{\partial^2 B_{ij}}{\partial u_p\partial u_q}+\frac{\partial^2 B_{ji}}{\partial u_p\partial u_q}\right)\cdot V_A\left(r_{ij}\right)\right.$$
$$-0.5\cdot\left(\frac{\partial B_{ij}}{\partial u_p}+\frac{\partial^2 B_{ji}}{\partial u_p}\right)\cdot\frac{\partial V_A\left(r_{ij}\right)}{\partial u_q}$$
$$+(-0.5)\cdot\left(\frac{\partial B_{ij}}{\partial u_q}+\frac{\partial^2 B_{ji}}{\partial u_q}\right)\cdot\frac{\partial V_A\left(r_{ij}\right)}{\partial u_p}$$
$$\left.-0.5\cdot\left(B_{ij}+B_{ji}\right)\cdot\frac{\partial^2 V_A\left(r_{ij}\right)}{\partial u_p\partial u_q}\right] \quad (54)$$

$$\left[\overline{\mathbf{K}}\right]=\frac{1}{2}\cdot\frac{\partial^2}{\partial\mathbf{u^2}}\left(V-\mathbf{F}^{\mathrm{T}}\mathbf{u}\right) \quad (55)$$

If a constant force field is applied on the system, Eq. (55) may be reduced to Eq. (54) and therefore:

$$\left[\overline{\mathbf{K}}\right]=\frac{1}{2}\cdot\frac{\partial^2 V}{\partial u_p\partial u_q} \quad (56)$$

In the equations above u_{i1}, u_{i2}, u_{i3} denote the coordinates of the i^{th} atom with respect to the global Cartesian CS with axes {1,2,3}, $\widehat{\mathbf{u_k}}$ denotes the unit vector along the k-axis of the global CS and u_n is the n^{th} degree of freedom of the total system. The relation between the atomic coordinate 'm' of the i^{th} atom and the equivalent DOF of the total system is given by $n=3\cdot i+m, m=\{1,2,3\}$